Renewable Energy 212 (2023) 415–429

Contents lists available at ScienceDirect

Renewable Energy

journal homepage: www.elsevier.com/locate/renene

Assessing the impact of wave model calibration in the uncertainty of wave energy estimation

Ajab Gul Majidi [a,b,*], Victor Ramos [a,b], Khalid Amarouche [c], Paulo Rosa Santos [a,b], Luciana das Neves [a,b], Francisco Taveira-Pinto [a,b]

[a] Department of Civil Engineering, Faculty of Engineering of the University of Porto (FEUP), Rua Dr. Roberto Frias, S/N, 4200-465, Porto, Portugal
[b] Interdisciplinary Centre of Marine and Environmental Research of the University of Porto (CIIMAR), Avenida General Norton de Matos, S/N, 4450-208, Matosinhos, Portugal
[c] Department of Civil Engineering, Faculty of Engineering of Bursa Uludağ University, 16240, Nilüfer, Bursa, Turkey

ARTICLE INFO

Keywords:
Wave energy converter
Wave modeling
Uncertainty analysis
Annual energy production
Atlantic coast

ABSTRACT

The accuracy of estimated sea conditions, specifically wave height and peak/average wave periods, affects the estimation of electrical energy production from wave energy converters. This study investigates the uncertainty in wave energy harvesting estimated by the SWAN wave model and determines possible improvements by adjusting the model's tunable parameters. Three different wave energy converters (OEBuoy, WaveBob, and Pontoon) and ten different locations along the Atlantic coast of the Iberian Peninsula are used in the study. The SWAN model is calibrated using the ST6 term package based on both wave height and peak period wave parameters. Different wave hindcast data produced by different model settings are used to estimate the wave energy produced by the wave energy converters at ten buoy locations and compared to wave energy produced estimated based on wave observations. The study finds that the physical settings of the SWAN model have a considerable influence on the uncertainty in the estimation of the power output produced by the device. The best-fitting calibrated model improved the mean energy output value of all locations compared to the SWAN default settings. The study concludes that adjusting the SWAN model parameters can improve the accuracy of the estimation of the energy output.

1. Introduction

Marine renewables and, in particular wave energy, are among the energy sources with the greatest potential to scale up and contribute to the ambitious European decarbonization targets to become the world's first climate-neutral continent by 2050, as stated in the EU's Green Deal [1], which implies decreasing the greenhouse gas (GHG) emission by 80–95%. In the past decade, the EU has endorsed an integrated approach to climate and energy policies, intending to fight climate change and increase the EU's energy security. These policies have been very successful in taking the first generation of renewable energy technologies, such as solar PV and wind, to commercially competitive levels. However, the EU will need other technologies to increase and diversify its low-carbon generation capacity in order to phase out the use of carbon-intensive fossil fuels and ensure a fair and just transition towards a more sustainable economy [2].

Over the last decade, the marine renewable energy sector has developed fast, especially in the field of offshore wind energy. Conversely, the wave energy sector is subject to continuous challenges. Despite the substantial progress achieved over this period, wave energy has not yet converged into a single/predominant technology [3], mainly because to date research and innovation on technology development and energy resource assessment have been mostly siloed. Surely, the potential of wave energy is indisputable, and the locations around the globe where the average power is particularly intense, are well known [4,5]. However, how can a promoter confidently assess which technology is the most appropriate for a specific location? Estimating the amount of electricity generated by a wave energy converter (WEC) in an area of interest is critical for determining the economic viability of a project. Furthermore, the energy output estimation must include several WECs to choose the best performing WEC for a given specific location

* Corresponding author. Department of Civil Engineering, Faculty of Engineering of the University of Porto (FEUP), Rua Dr. Roberto Frias, S/N, 4200-465, Porto, Portugal.
E-mail addresses: ajabgulmajidi@gmail.com (A.G. Majidi), jvrc@fe.up.pt (V. Ramos), amarouchekhalid@gmail.com (K. Amarouche), pjrsantos@fe.up.pt (P. Rosa Santos), lpneves@fe.up.pt (L. das Neves), fpinto@fe.up.pt (F. Taveira-Pinto).

https://doi.org/10.1016/j.renene.2023.05.049
Received 2 April 2023; Received in revised form 7 May 2023; Accepted 10 May 2023
Available online 18 May 2023

Abbreviations

[a1sds], [a2sds] Options in ST6 SWAN that can be used for wind scaling factor calibration
α high-frequency energy level estimated from JANSWAP project data
AEP Annual energy production
BIAS Bias
C_D Wind drag coefficient
cdfac A parameter in ST6 SWAN that can be calculated based on the wind stress and is used with the DEBIAS option
C_P phase speed at the peak frequency
c_θ Propagation velocity in θ space due to refraction
c_x The velocity of wave action density propagation in the x direction
c_y The velocity of wave action density propagation in the y direction
c_σ Propagation velocity in σ space due to variations in depths and impact of currents
DEBIAS An option available to the user in ST6 SWAN that can counter bias in the input wind fields by providing a multiplier on the drag coefficient
ECMWF European Centre for Medium-Range Weather Forecasts
ECMWF32 ECMWF wind drag formula with wind scaling factor of 32
ECMWF35 ECMWF wind drag formula with wind scaling factor of 35
E_0 Total energy output for the period of interest
ERA5 The fifth generation of the European Reanalysis
FAN Wind-Wave Model developed by Fabrice Ardhuin and Nicolas Rascle
FAN28 FAN wind drag formula with wind scaling factor of 28
FAN32 FAN wind drag formula with wind scaling factor of 32
FAN35 FAN wind drag formula with wind scaling factor of 35
g gravitational acceleration
GEBCO General Bathymetric Chart of the Oceans
GHG Greenhouse Gas
H_{m0} Significant wave height
Hwang Wind-Wave Model developed by Y.T. Hwang
HWANG32 HWANG wind drag formula with wind scaling factor of 32
HWANG35 HWANG wind drag formula with wind scaling factor of 35
JONSWAP Joint North Sea Wave Project
k Von Karman constant with a value of 0.4
MAE Mean absolute error
MIKE Hydrodynamic and Water Quality Model
nH Total number of wave height classes considered in the analysis
nT Total number of wave period classes considered in the analysis
NOAA National Oceanic and Atmospheric Administration
[p1sds], [p2sds] Options in ST6 SWAN that can be used for wind scaling factor calibration
P_{ij} Power generated by the WEC for a specific wave period and wave height
PTO Power take-off system
PV Photovoltaic
ρ_{ij} Percentage occurrence of wave energy
R Correlation coefficient
R_w logarithmic wind profile parameter
RMSE Root Mean Square Error
S_{bot} Shallow water source term: Bottom friction-induced dissipation
S_{brk} Shallow water source term: Wave breaking due to depth
S_{in} Deep-water source term: Energy transfer from the wind to waves
S_{nl3} Shallow water source term: Non-linear triad interaction
S_{nl4} Deep-water source term: Non-linear quadruplet wave-wave interactions
S_{tot} Total source term
S_{wc} Deep-water source term: Wave energy dissipation induced by whitecapping
SI Scatter Index
ST6 SWAN source term package
SWAN Simulating Waves Nearshore (a third-generation spectral wave model)
SWAN-DEF Default SWAN settings
ST6-DEF Default ST6 settings
T_e Wave energy period
T_p Peak wave period
T_{m02} Mean Zero-Crossing Period
TOMAWAC SWAN-based wave model for coastal and marine engineering applications
TRUE10 An option for wind scaling factor in ST6 SWAN
U_{10} 10-m wind speed
u_* friction velocity characterizing the shear stress at the surface
U10PROXY An option for wind scaling factor in ST6 SWAN that has been shown to improve the prediction of mean square slope
u_z wind speed at a particular height z above the surface
WAM A third-generation wave prediction model
WEC Wave Energy Converter
WWIII Wave Watch III Model
z a particular height above the surface
z_0 momentum roughness length that reflects the surface roughness's effect on the wind flow

[6]. Nonetheless, for this estimation to be meaningful, an accurate characterization of the wave potential is required [7,8]; otherwise, the cost-benefit calculation would be questionable.

Therefore, for the assessment of WECs, the necessary wave parameters must be obtained from a well-calibrated and validated numerical model for the area of interest. Among the different numerical tools to estimate the wave energy resource in the large ocean or coastal regions, the open-source SWAN spectral wave model has become one of the most popular options [9–11]. However, there are many tunable coefficients in the SWAN model that can be calibrated simultaneously and the most popular one is the whitecapping coefficient [12,13]. The ST6 terms package (considered the latest wave modeling calibration package [14]) can be parameterized with three different wind drag formulas, such as Hwang et al. [15], Fan et al. [16], and ECMWF [17]. Amarouche et al. [9], conducted sensitivity tests based on the tunable parameters recommended by the SWAN team [18] and concluded that the wind scaling factor and wind drag formulas are the most sensitive and influencing factors in the calibration of the ST6 source term package. In the present study, different wind scaling factors in HWANG, FAN, and ECMWF wind drag formulas of the operational SWAN ST6 source terms package (initially documented by Rogers et al. [19]), are used for the calibration of the model.

The wave energy resource must be accurately evaluated to obtain a credible estimation of the power output of wave energy farms [20]. For instance, Hiles et al. [21] investigated the uncertainty in the estimation of the power output of wave farms using data from simulated

deployments of WECs with different working principles in different locations. For this purpose, a Monte Carlo method was used to analyze the mean Annual Energy Production (AEP) and it showed uncertainty levels ranging from 2% to 20%. It was also found that the type of WECs and deployment location had a significant impact on the obtained uncertainty levels, which were also highly sensitive to the number of input data [21]. In addition, several researchers, such as Livermore [22] using the standard error propagation method (a similar approach to that applied in wind energy), Guanche et al. [23] using a boot-strap resampling technique, Mackay et al. [24] investigating the impacts of sampling variability method, Kofoed et al. [25], and Bailey et al. [26], propose different methods to estimate the uncertainty of the mean AEP associated with the WEC performances.

In consequence, one of the challenges for the wave energy industry to overcome is to develop fair and consistent methodologies for evaluating the performance of WEC technologies. For this purpose, the International Electrotechnical Commission developed and regularly updates technical specifications to homogenize and standardize the key aspects related to wave energy resource assessment and WEC performance assessment [27,28]. However, there are uncertainties from a range of contributing factors when a performance matrix is used together with calculations based on observed data from a deployed WEC at a single location [21,29].

The AEP is usually calculated using the WEC power matrix obtained experimentally or numerically by WEC developers. Another component used in the AEP computation is the wave resource matrix, which presents the probability of occurrence of each sea state and should be prepared according to the power matrix of the WEC device. The wave energy resource matrix can be elaborated using wave data obtained from either field measurements or numerical modeling (e.g., SWAN [18], MIKE [30], TOMAWAC [31], WWIII [32], and WAM [33]). In the case of using data from numerical modeling, the shape of the wave resource matrix can be highly influenced by the set-up of the main physical parameters of the wave model. These changes may shift the number of events from one class to another (from one cell to another) and, hence, their probability will be multiplied by a different cell in the power matrix, having a different power conversion value.

Therefore, a notable uncertainty may occur when estimating the power output using the power matrix of WEC technologies. For this reason, the present study focuses on investigating the impacts of the adjustment of the physical parameters of the SWAN wave model on the estimation of the energy production of WECs. For this purpose, the OEBuoy, WaveBob, and Pontoon [34,35] technologies were used as case studies in combination with 10 different locations alongside the Atlantic coast of the Iberian Peninsula. This region, facing the North Atlantic, presents one of the most energetic wave regimes in continental Europe [36–39], and, therefore, it appears as a promising location for the exploitation of the wave energy resource.

The remainder of this paper is structured as follows: Section 2 describes the physics of the SWAN numerical model and the input and calibration factors considered for this work. Section 3 presents a brief description of the WEC technologies analyzed in this research work. Section 4 presents and discusses the results obtained. Finally, conclusions are drawn in Section 5.

2. SWAN numerical model

2.1. SWAN physics

SWAN is a third-generation spectral wave model developed at the Delft University of Technology (Netherlands) and is available through an open-source license. The SWAN model is among the most widely used wave models on a regional scale [40–44] and has been properly implemented on a global scale. SWAN uses an Eulerian formulation of the balance of wave energy densities to compute variations in wave action density (N) [45].

$$\frac{\partial}{\partial t}N+\frac{\partial}{\partial x}c_xN+\frac{\partial}{\partial y}c_yN+\frac{\partial}{\partial \sigma}c_\sigma N+\frac{\partial}{\partial \theta}c_\theta N=\frac{S_{tot}}{\sigma}, \quad (1)$$

where the first term represents the local rate of change in wave action density in time, and the second and third terms represent the propagation of wave action density in the geographical space with velocities of c_x and c_y in the x and y directions, respectively. The fourth term is the shifting of the relative frequency with a propagation velocity c_σ in σ space due to variations in depths and the impact of currents. The fifth term is the refraction due to currents and bathymetry changes with a propagation velocity c_θ in θ space [46,47]. The generation, dissipation, and redistribution of wave energy are all represented on the right side of Eq. (1). Eq. (2) shows the six deep and shallow water source and sink terms that may be used to simulate wind-to-wave energy transfer and wave energy dissipation [48]:

$$S_{tot}=S_{in}+S_{wc}+S_{nl4}+S_{bot}+S_{brk}+S_{nl3}, \quad (2)$$

where the deep-water source terms refer to an energy transfer from the wind to waves (S_{in}), wave energy dissipation induced by whitecapping (S_{wc}), and non-linear quadruplet wave-wave interactions (S_{nl4}). On the other hand, bottom friction-induced dissipation (S_{bot}), wave breaking due to depth (S_{brk}), and non-linear triad interaction (S_{nl3}) terms are the shallow water source terms [49]. Consequently, SWAN simulates wind-wave generation, dissipation, and propagation, including the effects of shoaling and refraction from depths and currents, triad- and quad-wave interactions, bottom friction, whitecapping dissipation, and refraction due to water depth variations and diffraction effects.

In order to simulate energy transmission to, from, and between waves, each of the abovementioned parameterizations relies on laboratory and experimental data. In this context, the ST6 physics package was added with SWAN release version 41.20, including, among others, parameterizations for wind input, whitecapping, wind speed scaling, and swell dissipation. Similarly, wave models (*e.g.* NOAA's WaveWatch III) have also integrated the ST6 physics package. The whitecapping term, S_{wc}, has two main assumptions in the expression used in ST6 [50]: firstly, waves do not break unless the spectral density at a particular frequency exceeds a threshold calculated from the spectral saturation spectrum. Secondly, two separate dissipation terms for the two phases of the whitecapping term are assumed to be distinguishable based on two distinct mechanisms [51].

The level of roughness on the surface of the ocean is significant in its interaction with the atmosphere. This is primarily because it causes resistance to the wind, which in turn has an impact on the exchange of mass, momentum, and energy between the ocean and the atmosphere [15]. Rogers et al. [19], offered a modified equation based on [52] for the ST6 wind input term in the SWAN model, which included a negative input term owing to oblique and unfavorable winds.

2.2. The ST6 physics

The ST6 package is a physics module in the SWAN wave model that computes the source terms of waves, including those generated by wind, currents, and wave-wave interactions. The wind source term is computed using a wind scaling factor and a wind drag formula. The wind scaling factor adjusts the wind speed to the height of the wave boundary layer and is determined by the [windscaling] option. The wind drag formula is used to calculate the drag coefficient, which, in turn, is used to calculate the wind stress on the sea surface. The ST6 module offers the options of HWANG [15], FAN [16], and ECMWF [17] drag formulas, with HWANG [15] being the default option that is recommended for use with the DEBIAS option, which corrects for bias in the input wind fields.

Moreover, the ST6 package includes a wave-wave interaction source term that accounts for the transfer of energy between different wave components. The wind scaling factor and wind drag formulas are

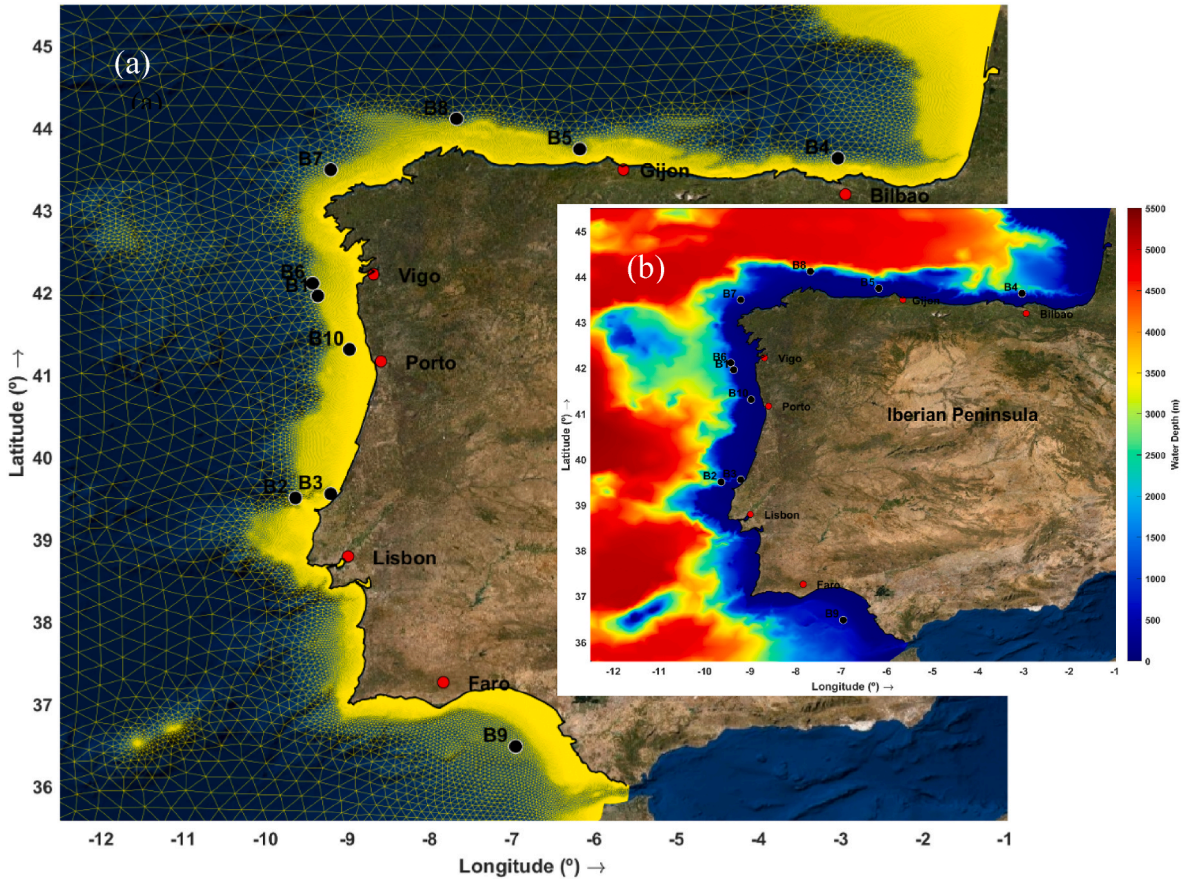

Fig. 1. The defined unstructured mesh grid system (a), bathymetry (b), and buoy locations (black dots) for the study area.

considered the most sensitive and influential factors in the calibration of the ST6 source term package. The wind scaling factor is defined as the ratio of the wave height to the wind speed, and the user can choose from a selection of calibrated options, including [a1sds], [a2sds], [p1sds], and [p2sds]. The user can also choose between the TRUE10 and U10PROXY options for the wind scaling factor, with the default option being U10PROXY with [windscaling] = 32, which has been shown to improve the prediction of the mean square slope. The DEBIAS option is another choice available to the user, which can counter bias in the input wind fields by providing a multiplier on the drag coefficient [53]. The physics of the ST6 module are described in detail in Rogers et al., [19].

The wind drag coefficient (C_D) defined by Hwang et al. [14,15,19] is given in Eq. (3).

$$C_D = 10^{-4} \times \left(8.058 + 0.967U_{10} - 0.016U_{10}^2\right), \tag{3}$$

Where, U_{10} is the 10-m wind speed. The wind drag coefficient defined by Fan et al. [16] is computed by the following equations

$$C_D = 10^{-3} \times \left(0.021 + \frac{10.4}{R_w^{1.23} + 1.85}\right), \tag{4}$$

$$R_w = \ln\left[\frac{zg}{0.2\sqrt{\alpha u_z}}\right], \tag{5}$$

where g is gravitational acceleration, α is the high-frequency energy level estimated parametrically from JANSWAP project data and given by the following equation.

$$\alpha = 0.57\left(\frac{C_P}{u_*}\right)^{-1.5}, \tag{6}$$

$$u_z = \frac{u_*}{k} ln\left(\frac{z}{z_0}\right), \tag{7}$$

where C_P is the phase speed at the peak frequency, u_z represents the wind speed at a particular height z above the surface, u_* is the friction velocity that characterizes the shear stress at the surface, k is a constant with a value of 0.4 known as the Von Karman constant, and z_0 represents the momentum roughness length that reflects the surface roughness's effect on the wind flow.

The wind drag coefficient of ECMWF followed by WAM cycle 4 based on Janssen [17] is given in Eq. (7).

$$C_D = \begin{cases} 1.2875\times10^{-3}, U_{10} < 7.5\ m/s \\ (0.8 + 0.065U_{10}) \times 10^{-3}, U_{10} \geq 7.5\ m/s \end{cases} \tag{8}$$

In the present study, a comparison of SWAN default, ST6 default, Hwang wind drag formula with wind scaling factors of 32 and 35, FAN wind drag formula with wind scaling factors of 28, 32, and 35, and ECMWF wind drag formula with wind scaling factors of 32 and 35, has been carried out for the area of study.

2.3. SWAN model implementation

The most important input parameter affecting the wind-wave modeling accuracy is wind forcing [54]. In the present study, the wave model is forced with hourly ERA5 wind reanalysis, which presents a spatial resolution of 0.25 × 0.25° [55]. The ERA5 wind data is produced by the European Center for Medium-Range Weather Forecasts (ECMWF) using an integrated forecast system consisting of 137 sigma-pressure hybrid layers with a 0.01 hPa top-level [56]. The ERA5 wind data is currently among the most widely used wind reanalysis

Table 1
Location, buoy ID, water depth, and number of data records available in 2010 for all the considered locations.

Location	Buoy ID	Lon (°)	Lat (°)	Depth (m)	Data No
B1	6200084	−9.3675	41.9665	292.5	4996
B2	6200192	−9.64	39.51	1547.1	2629
B3	6200199	−9.21	39.56	65.4	2214
B4	2136	−3.04	43.64	827.0	8513
B5	2242	−6.18	43.75	748.0	6020
B6	2248	−9.43	42.12	691.3	4996
B7	2246	−9.21	43.5	424.8	8726
B8	2244	−7.68	44.12	1650.0	1160
B9	2342	−6.96	36.49	467.0	6863
B10	Leixões Buoy	−8.983	41.3167	84.8	2524

datasets in wind-wave climate studies [57] and it is considered a reference for the validation and improvement of historical and future climate projections [58]. In this sense, several studies have confirmed the accuracy of the ERA5 wind data in different areas around the world [9,59–62]. SWAN can compute wave propagation using regular, curvilinear, or unstructured computational grids based on cartesian or spherical coordinate systems [48,63,64]. In this study, in order to catch the critical effect of local physics without sacrificing computational efficiency, an unstructured grid system is used (Fig. 1a). The unstructured grid presents a space varying cell size, which ranges from 0.002° (0.25 km) to 0.26° (29 km) in the present study. As a result, the grid consists of 114518 vertices, 220485 internal cells, 4261 boundary cells, 334975 internal faces, and 4288 boundary faces. The bathymetry dataset (Fig. 1b) interpolated onto the grid was obtained from the General Bathymetric Chart of the Oceans (GEBCO) [65].

The wave boundary conditions for the model were extracted from the hourly ERA5 wave hindcast reanalysis [55], which presents a 1 × 1° spatial resolution alongside the area of the study (Fig. 1a and b). The model was run in non-stationary mode and the boundary conditions were imposed using a JONSWAP spectrum, which was defined in terms of significant wave height (H_{m0}), peak wave period (T_p), and peak wave direction (Θ_P). Following previous works on the area of study, the JONSWAP spectrum peak enhancement factor was set to 3.3 [38]. Finally, it is worth mentioning that the model was calibrated against the measurements of 10 wave buoys operated either by the Portuguese Hydrographic Institute or by the Spanish Port Authority, Table 1.

3. Case-study WECs

The OEBuoy, WaveBob, and Pontoon technologies were selected for evaluating the uncertainties in the energy output due to the SWAN model set-up. The three selected WECs are all point absorbers, whose operating characteristics make them suitable to operate at the locations where the wave buoys indicated in Table 1 are located.

OEBuoy is a floating oscillating water column, which keeps an air pocket fixed just above the water column in a semi-submerged open chamber below the ocean free surface. Incoming waves cause the oscillating water column to move up and down. The produced airflow passes through a bidirectional turbine that converts its energy into electrical energy. OEBuoy presents a rated power output of 2880 kW. In its power matrix (Appendix A, Table A1), the power output rises until a maximum operational significant wave height (H_{m0}) of 7 m. In terms of wave period, power production reaches its maximum at an operational peak period (T_p) of 11 s and then falls back. Only 3% of the operational H_{m0} and T_p combinations have a power conversion above 80% of the WEC rated power [26].

WaveBob is an axisymmetric self-reactive point absorber made of a torus sliding along a vertical floating body connected to a high-inertia underwater tank. A hydraulic Power Take-Off (PTO) system generates power by the relative motions between the two bodies, having a rated power of 1000 kW. Its power matrix has a wide power band (Appendix A, Table A2) and roughly 13% of the operating H_{m0} and T_p combinations have a power conversion above 80% of the WEC nominal power [35].

The Pontoon WEC is a multiple-point absorber made up of numerous heaving buoys connected by a hydraulic PTO system to a common

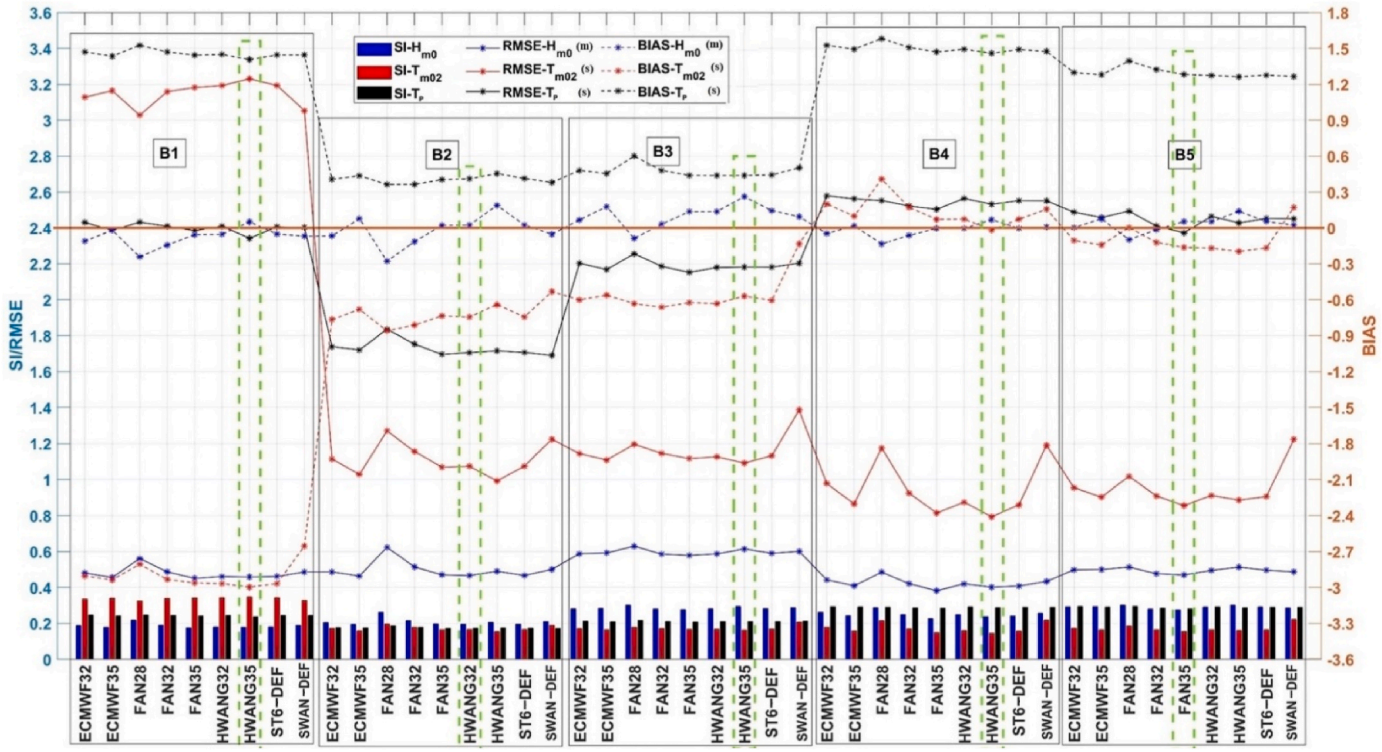

Fig. 2. Changes of *SI*, *RMSE*, and *BIAS* (dash-lines) error parameters of H_{m0} (blue), T_{m02} (red), and T_p (black) of 9 different SWAN settings for the locations B1, B2, B3, B4, and B5. The left y-axis represents both the *SI* and *RMSE* and the right y-axis represents the *BIAS*.

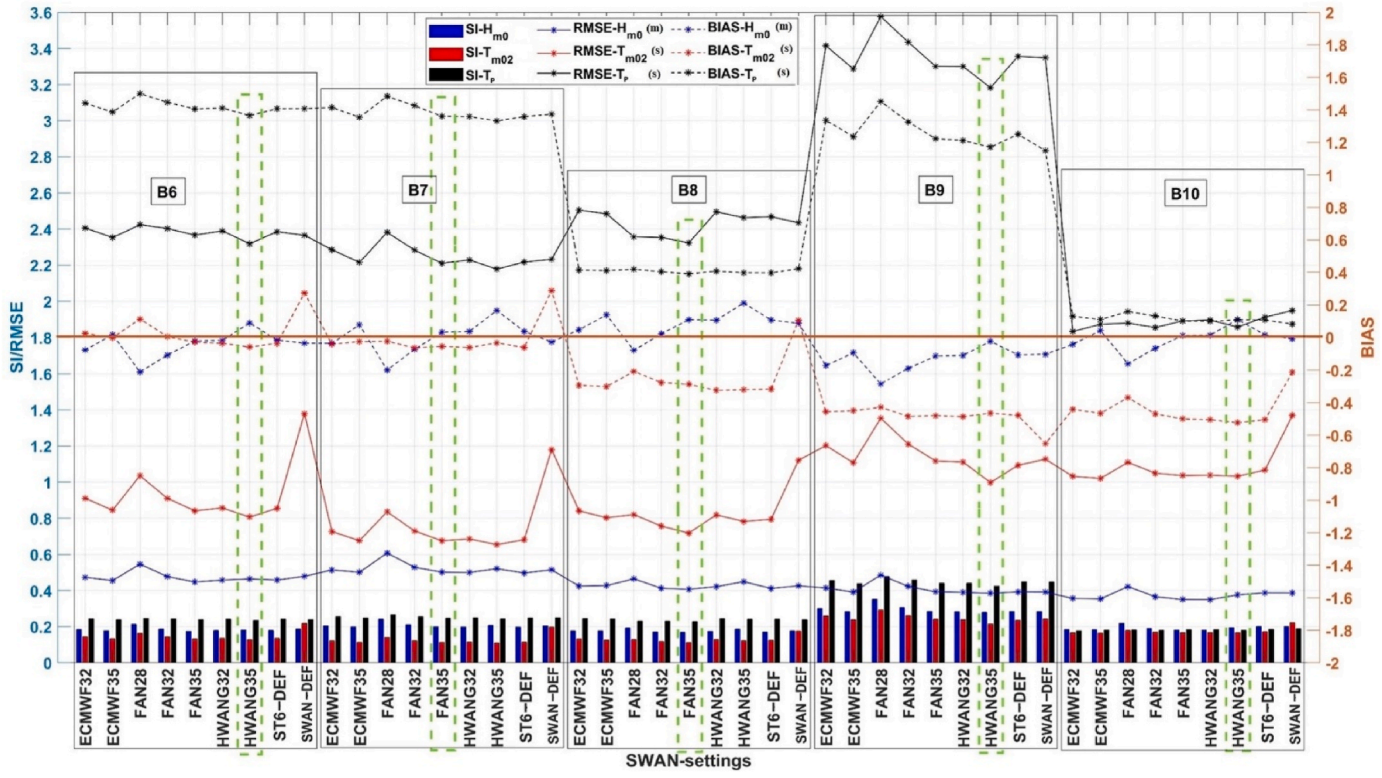

Fig. 3. Changes of *SI*, *RMSE*, and *BIAS* (dash-lines) error parameters of H_{m0} (blue), T_{m02} (red), and T_p (black) of 9 different SWAN settings for the locations B6, B7, B8, B9, and B10. The left y-axis represents both the *SI* and *RMSE* and the right y-axis represents the *BIAS*.

underwater structure. The Pontoon unit considered in this work includes 10 heaving buoys and has a nominal power of 3619 kW. Because the device cannot perform well in both short and long-crested waves, only 12% of the bins in the power matrix have a normalized power output above 40% of its nominal power (Appendix A, Table A3) [35].

4. Results and discussion

4.1. SWAN model calibration

One of the main objectives of this study is to calibrate the implemented wave model by adjusting the ST6 SWAN package settings. Recently, several studies [9,13,14,66] showed that the use of the new ST6 package in the SWAN model provides better accuracy than the

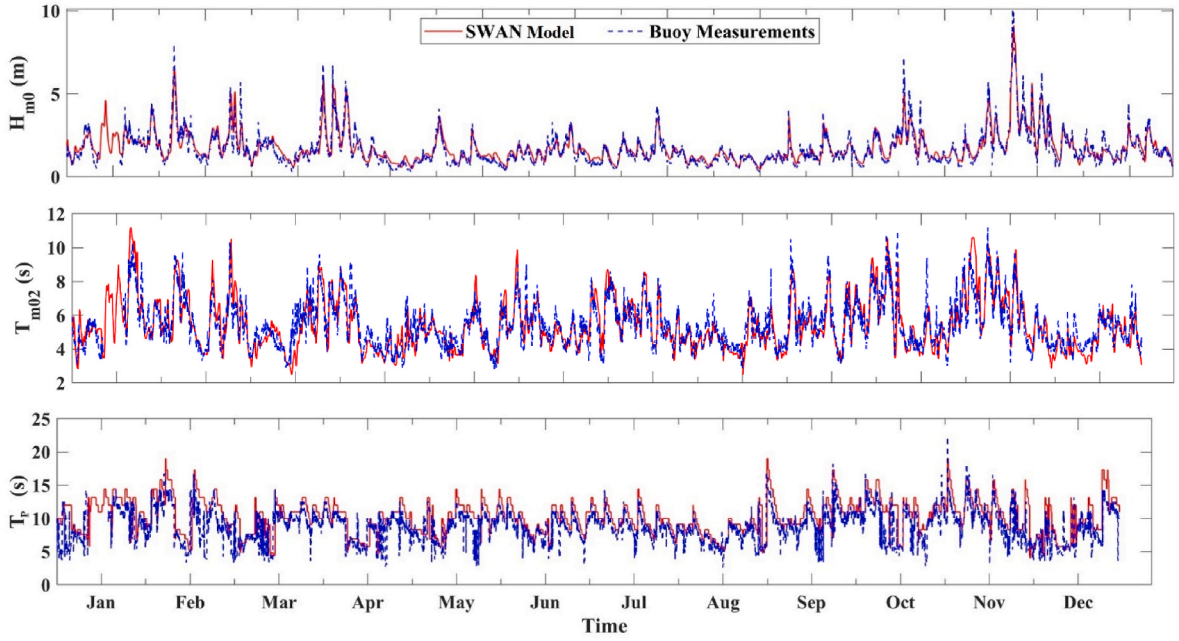

Fig. 4. Time series of H_{m0}, T_{m02}, and T_p of the SWAN model (HWANG35) against the measurements from buoy B4 for the year 2010.

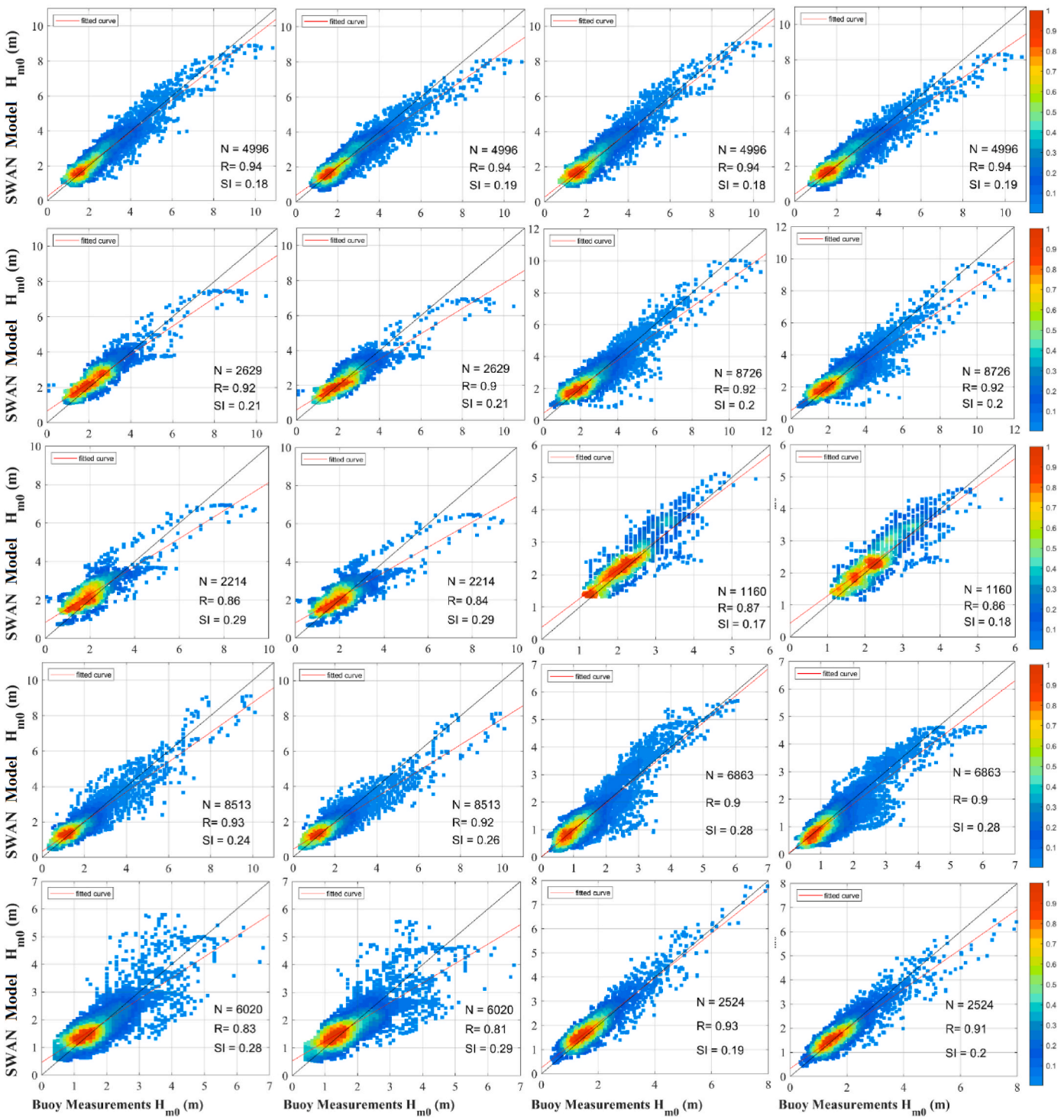

Fig. 5. A comparison of the scatter diagrams for H_{m0} between the SWAN default and the calibrated model for all 10 different locations considered in the study area.

default SWAN settings. Thus, the ST6 package was calibrated by adjusting the wind drag formulation, wind scaling factor, and wind growth formula. For this purpose, a detailed comparison of the SWAN default (SWAN-DEF), ST6 default (ST6-DEF), HWANG with wind scaling factors of 32 (HWANG32) and 35 (HWANG35), FAN with wind scaling factors of 28 (FAN28), 32 (FAN32), and 35 (FAN35), ECMWF with wind scaling factors of 32 (ECMWF32) and 35 (ECMWF35) has been carried out. The outputs of these 9 different SWAN settings are compared against measurements of 10 different wave buoys alongside the area of interest (Table 1). To assess the performance of each SWAN setting across the study area, the scatter index (SI), Root Mean Square Error (RMSE), and *BIAS* have been computed for the wave spectral parameters (H_{m0}, T_{m02}, and T_p) for the locations highlighted in Table 1. The results obtained are plotted in Figs. 2 and 3. Evaluating the 9 different error parameters (*SI-*H_{m0}, *SI–*T_{m02}, *SI-*T_p, *RMSE-*H_{m0}, *RMSE-*T_{m02}, *RMSE-*T_p, *BIAS-*H_{m0}, *BIAS-*T_{m02}, *BIAS-*T_p), at all 10 locations, in overall, it can be concluded that HWANG35 presents the best performance except for locations B5, B7, and B8, where FAN35 shows the lowest error values (Figs. 2 and 3).

The time series for the significant wave heights (H_{m0}), mean wave

Table 2
R, *BIAS*, *RMSE*, *MAE*, and *SI* statistical error parameters for the H_{m0}, T_{m02}, and T_p of 10 different buoy measurements against SWAN-DEF and HWANG35 model settings around the study area.

Model/Location		N	H_{m0} (m)					T_{m02} (s)					*TP* (s)				
			R	*BIAS* (m)	*RMSE* (m)	*MAE* (m)	SI	R	*BIAS* (s)	*RMSE* (s)	*MAE* (s)	SI	R	*BIAS* (s)	*RMSE* (s)	*MAE* (s)	SI
HWANG35	**B1**	4996	0.94	0.05	0.46	0.35	0.18	0.80	−3.00	3.23	3.00	0.35	0.66	1.41	2.35	1.83	0.24
	B2	2629	0.92	0.19	0.49	0.38	0.21	0.82	−0.64	0.99	0.75	0.15	0.75	0.45	1.72	1.17	0.17
	B3	2214	0.86	0.26	0.62	0.49	0.29	0.77	−0.57	1.09	0.85	0.16	0.63	0.44	2.18	1.46	0.21
	B4	8513	0.93	0.07	0.40	0.29	0.24	0.86	−0.02	0.79	0.59	0.15	0.67	1.46	2.54	1.83	0.29
	B5	6020	0.82	0.14	0.51	0.37	0.30	0.71	−0.20	0.89	0.65	0.16	0.56	1.26	2.43	1.79	0.29
	B6	4996	0.94	0.09	0.46	0.36	0.18	0.85	−0.06	0.81	0.60	0.13	0.66	1.37	2.33	1.81	0.24
	B7	8726	0.92	0.17	0.52	0.39	0.21	0.88	−0.03	0.65	0.49	0.11	0.72	1.33	2.19	1.63	0.24
	B8	1160	0.88	0.21	0.45	0.36	0.19	0.84	−0.32	0.78	0.57	0.12	0.57	0.40	2.48	1.66	0.24
	B9	6863	0.90	−0.02	0.39	0.28	0.28	0.82	−0.46	1.00	0.77	0.22	0.63	1.17	3.19	2.25	0.42
	B10	2524	0.93	0.11	0.38	0.30	0.19	0.79	−0.52	1.03	0.78	0.17	0.72	0.11	1.86	1.15	0.18
	ABS mean	**4864**	**0.90**	**0.13**	**0.47**	**0.36**	**0.23**	**0.81**	**−0.58**	**1.13**	**0.91**	**0.17**	**0.66**	**0.94**	**2.33**	**1.66**	**0.25**
SWAN-DEF	**B1**	4996	0.94	−0.07	0.49	0.36	0.19	0.73	−2.65	3.05	2.67	0.33	0.65	1.45	2.40	1.85	0.24
	B2	2629	0.90	−0.05	0.50	0.36	0.21	0.77	−0.53	1.22	0.96	0.19	0.77	0.38	1.69	1.12	0.17
	B3	2214	0.84	0.09	0.60	0.46	0.29	0.71	−0.13	1.39	1.10	0.21	0.63	0.50	2.20	1.44	0.21
	B4	8513	0.92	0.01	0.43	0.31	0.26	0.78	0.16	1.19	0.91	0.22	0.67	1.47	2.55	1.84	0.29
	B5	6020	0.81	0.02	0.49	0.36	0.29	0.63	0.17	1.22	0.97	0.22	0.56	1.27	2.45	1.79	0.29
	B6	4996	0.94	−0.04	0.48	0.36	0.19	0.80	0.27	1.38	1.10	0.22	0.66	1.41	2.37	1.82	0.24
	B7	8726	0.92	−0.03	0.51	0.36	0.20	0.82	0.29	1.18	0.90	0.20	0.71	1.37	2.23	1.64	0.25
	B8	1160	0.86	0.09	0.43	0.33	0.18	0.79	0.11	1.12	0.85	0.18	0.59	0.42	2.44	1.64	0.24
	B9	6863	0.90	−0.10	0.39	0.28	0.28	0.81	−0.65	1.13	0.92	0.24	0.60	1.15	3.35	2.39	0.45
	B10	2524	0.91	−0.01	0.39	0.28	0.20	0.73	−0.21	1.37	1.08	0.22	0.69	0.08	1.95	1.21	0.19
	ABS mean	**4864**	**0.89**	**0.05**	**0.47**	**0.35**	**0.23**	**0.76**	**0.52**	**1.43**	**1.15**	**0.22**	**0.65**	**0.95**	**2.36**	**1.67**	**0.26**

periods (T_{m02}), and peak periods (T_p) for the HWANG35 SWAN setting against the measurements from buoy B4 for the year 2010 are presented in Fig. 4. These time series clearly show that the SWAN model can estimate those wave parameters satisfactorily. Overall, it can be concluded that the higher values of H_{m0} (top panel) are underestimated whereas the lower values are overestimated. However, in T_{m02} (middle panel), the higher values are overestimated, and the lower values of the model are underestimated. Finally, the T_p (bottom panel) is slightly overestimated in the time frame of 2010.

For a better understanding of the model performance, the scatter diagrams of H_{m0} for all the considered SWAN settings against 10 different in-situ measurements are presented in Fig. 5. Each figure contains a red and a black line that highlights the clustering of data points. The red line represents the best-fitted curve, and the black line shows the regression model y = cx. N is the number of temporally matched data in the dataset. In general terms, the scatter diagrams of H_{m0} confirm the model accuracy. Again, for all the locations analyzed, the best-fitted curves show overestimations and underestimations in the low and high values of H_{m0}, respectively.

After analyzing the results, it is observed that the HWANG35 setting provides the closest values to the data from buoy measurements for 7 different locations (B1, B2, B3, B4, B6, B9, and B10) and the FAN35 setting for 3 (B5, B7, and B8).

For the validation of the best model setting, some statistical error parameters such as *N*, *R*, *BIAS*, *RMSE*, *MAE*, and *SI*, for H_{m0}, T_{m02}, and T_p are presented in Table 2. The error parameters in Table 2 are improved in the adjusted model compared to the default model, but this improvement is much more significant in T_{m02} and T_p. The equations used to determine the statistical error parameters are presented in Appendix B.

4.2. The energy output of the case-study WECs

In this section, the uncertainties in terms of AEP estimation are investigated for the three case-study WECs (OEBuoy, WaveBob, and Pontoon). For this purpose, the measured and modeled (considering the different ST6-SWAN settings) wave conditions are used to construct the omnidirectional wave energy resource matrices for the locations highlighted in Table 1. Then, the wave resource matrices are combined with the power matrices of the WECs to compute the AEP. Finally, a comparison of the AEP estimated using the model results and the field measurements is carried out. The matched datasets between the model and measurements are classified considering the characteristics (H_{m0} and T_p steps) of the power matrix of OEBuoy, WaveBob, and Pontoon. The results show that the model accuracy changes depending on the sea state conditions. Since the best results for 70% of the investigated locations were obtained using HWANG35 and location B4 has the largest data record entries among the 7 best-fitted locations with HWANG35, location B4 is here discussed in more detail. The difference in the number of events between the resource matrices obtained from the SWAN model and measurements for location B4 are given in Table 3.

The model underestimates the occurrences for sea states in the range from 0.5 to 5.5 m of H_{m0} and 2–9 s of T_p. Conversely, the model overestimates the occurrence of sea states concentrated in the region between 1 and 5 m of H_{m0} and 11–16 s of T_p. Consequently, the results show that the sea states estimated by the SWAN model are shifted from the lower T_p bins to the higher T_p bins.

Using the power matrix of OEBuoy (Appendix A, Table A1) and the wave energy resource matrices obtained from the SWAN simulations and buoy measurements for location B4, and applying Eq. (9), the energy output for each sea state can be calculated (Tables 4 and 5, respectively). Due to the lack of continuous measurements available in location B4 during the year 2010, the energy during a period of 8513 h (approximately one year). The total energy output for the period of interest, E_0, can be calculated using,

$$E_0 = \sum_{i=1}^{nT} \sum_{j=1}^{nH} \rho_{ij} \times P_{ij} \times \Delta\,\mathrm{T} \tag{9}$$

where ρ_{ij} represents the percentage occurrence of wave energy, and P_{ij} represents the power generated by the WEC for a specific wave period (*i*th class) and wave height (*j*th class). The value of ρ_{ij} is obtained from the wave scatter diagram calculated over the period Δ T at the chosen location, while the P_{ij} is obtained from the power matrix of the WEC. The values of *nT* and *nH* represent the total number of wave period and wave height classes, respectively, that were considered in the analysis [67].

Table 3
Differences in the number of events (hours) between the resource matrices obtained from the SWAN model (HWANG35) and measurements for specific H_{m0} (m) and T_p (s) intervals in B4.

H_{m0} (m)	T_p (s)																						
	0	1	2	3	4	5	6	7	8	9	10	11	12	13	14	15	16	17	18	19	20	21	22
0.0	0	1	−1	−3	−2	2	−4	−11	−21	−11	−6	−2	0	0	0	0	0	0	0	0	0	0	0
0.5	0	0	−9	−103	−75	−115	13	−100	−192	−82	8	−133	41	26	−10	0	−2	0	0	0	0	0	0
1.0	0	0	0	−43	−126	−129	30	1	−145	−1	635	−239	356	162	60	33	−13	12	10	0	0	0	0
1.5	0	0	0	−2	−42	−141	−78	18	−12	−19	330	−231	335	212	25	23	−2	21	4	0	0	0	−1
2.0	0	0	0	0	−2	−47	−61	−105	18	−39	48	−187	69	179	20	27	−15	14	3	0	0	0	0
2.5	0	0	0	0	0	−13	−53	−100	4	−3	−15	−99	−4	70	52	42	−7	13	2	0	0	0	0
3.0	0	0	0	0	0	0	−10	−45	−14	−9	25	−51	15	22	23	23	−2	5	0	0	0	0	0
3.5	0	0	0	0	0	0	−1	−11	−17	−10	38	−39	−4	14	7	14	−2	4	0	0	0	0	0
4.0	0	0	0	0	0	0	0	−3	−7	−9	−1	−32	11	30	15	0	0	0	0	0	0	0	0
4.5	0	0	0	0	0	0	0	0	−2	−5	1	−27	−12	14	15	6	−1	0	0	0	0	0	0
5.0	0	0	0	0	0	0	0	0	−2	−3	4	−4	0	6	−6	3	0	0	0	0	0	0	0
5.5	0	0	0	0	0	0	0	0	0	−1	0	−14	−7	−1	1	3	0	0	0	0	0	0	0
6.0	0	0	0	0	0	0	0	0	0	0	−2	−2	0	0	3	4	0	0	0	0	0	0	0
6.5	0	0	0	0	0	0	0	0	0	0	−4	−4	0	1	−3	8	−5	0	0	0	0	0	0
7.0	0	0	0	0	0	0	0	0	0	0	−1	0	−1	0	−8	2	−1	0	0	0	0	0	0
7.5	0	0	0	0	0	0	0	0	0	0	0	0	0	−1	0	4	0	0	0	0	0	0	0
8.0	0	0	0	0	0	0	0	0	0	0	0	−1	−1	−1	0	6	0	0	0	0	0	0	0
8.5	0	0	0	0	0	0	0	0	0	0	0	0	−2	0	0	7	0	0	0	0	0	0	0
9.0	0	0	0	0	0	0	0	0	0	0	0	0	0	−2	−1	4	0	0	0	0	0	0	0
9.5	0	0	0	0	0	0	0	0	0	0	0	0	0	0	0	−3	−1	0	−4	0	0	0	0
10.0	0	0	0	0	0	0	0	0	0	0	0	0	0	0	−1	0	0	0	0	0	0	0	0

It can be concluded that when real buoy measurements are considered (Table 5), the energy output is concentrated between 7 and 12 s of T_p and 1–4 m of H_{m0}, whereas for SWAN model outputs (Table 4) it is mostly concentrated between 9 to 11 s and 12–14 s of T_p and 1.5–3 m of H_{m0}. These results are linked to the shift, in SWAN model simulation outputs, of some sea states from lower T_p-valued cells to higher T_p-valued cells while others sea states shifted from higher T_p-valued cells to lower T_p-valued cells in the resource matrix. Meaning that the model accuracy is lower for T_p compared to H_{m0}. The differences in the energy output in MWh, from the SWAN model (Table 4) and real measurements (Table 5) based estimations, are given in Table 6.

Table 6 shows that model-based assessments overestimate the energy produced for higher T_p values and underestimate the energy harvested by the WEC in the ranges of lower T_p values.

The total energy output produced by OEBuoy for the 10 locations around the study area, obtained from the wave measurements and 9 different SWAN model settings, are presented in Table 7. Overall, HWANG35 SWAN settings presents the nearest results to the wave measurement outputs, except for locations B2 with FAN35, B3 and B8 with FAN32, and B10 with SWAN-DEF. The averages of all locations (Table 7) show that HWANG35, with 1439.21 MWh of energy output, has the closest result to the energy output based on real measurements (1404.3 MWh). Due to the availability of the buoys measurements, the energy outputs for most of the buoys are not exactly AEPs, since they only cover a portion of the year 2010 (except for B7 and B4), which is given in column T (YEAR) of Table 7.

The differences (in percentage) between the energy output of the model and the measurements for all the considered 10 locations and 9 different SWAN adjustments for OEBuoy, WaveBob, and Pontoon, are presented in Tables 8–10, respectively. The mean values in those tables were calculated from the mean energy output of the model and the in-situ measurement from all 10 locations (data in Table 7 was used).

HWANG35 presented the lowest error percentages for OEBuoy (Table 8) in locations B1, B4, B6, B7, and B9. The average deviation for all 10 locations was 2.5%. Locations B2 (0.39%) with FAN35, B3 (0.16%) with FAN32, B8 (3.33%) with FAN32, and B10 (−0.98%) with SWAN-DEF presented the lowest differences in the total energy output compared to the in-situ measurements. For WabeBob (Table 9), results suggest similar SWAN adjustments for all locations except for B8, which changed from FAN32 to FAN28 settings (−1.48% difference), and B10 which changed from SWAN-DEF to HWANG32 settings (0.63% difference). The Pontoon (Table 10) presented less total energy output differences for more locations with the HWANG35 settings compared to OEBuoy and WaveBob. In fact, only B3 with ST6-DEF (−0.37%), B8 with ECMWF32 (−0.56%), and B10 with HWANG32 (0.68%) are not performing well with HWANG35 SWAN adjustment. When looking at the averages, HWANG35 settings present the best results, having the lowest errors for all considered WEC devices which, roughly, presents an agreement with the SWAN model calibration presented in Figs. 2 and 3.

Considering the results obtained from the current study, it is understood that the calibrated SWAN model usually gives the closest results to the actual measurements with the HWANG35 model setting. To highlight this, Table 11 presents the SWAN setting that leads to the energy output closer to that obtained from the real measurements, for the three considered WECs and for all the 10 locations.

Locations B2, B3, B8, and B10, with fewer wave measurements, generally showed different SWAN settings for different WEC technologies in different locations. The reason for this variability could be the number of wave data available, but for location B7, which was a full year of wave data, the best SWAN calibration is FAN35 while for all case study WECs the HWANG35 settings present the best results. If we look at location B7, it can be observed that the difference in the energy output of all case study WECs is higher than 7% (optimal SWAN calibration setting (FAN35) vs the calibration setting recommended by the energy output of the case study WECs (HWANG35)). These outcomes confirm that in the assessment of a WEC device in a particular location, it is extremely

Table 4
Energy output matrix (MWh) obtained for OEBuoy and location B4, considering HWANG35 settings.

	T_p (s)												
H_{m0} (m)	**4**	**5**	**6**	**7**	**8**	**9**	**10**	**11**	**12**	**13**	**14**	**15**	**16**
1.0	0.3	1.4	3.0	4.7	5.3	7.5	11.0	5.7	1.7	2.2	0.6	0.0	0.0
1.5	0.3	5.8	16.1	21.3	26.2	47.3	86.6	49.5	20.2	27.3	11.4	4.9	1.1
2.0	0.0	1.6	9.6	23.5	37.2	45.1	88.4	57.7	32.0	47.9	20.8	5.1	1.4
2.5	0.0	0.3	4.0	15.4	36.6	36.2	45.5	30.2	17.7	39.2	27.2	7.4	2.5
3.0	0.0	0.0	1.1	5.6	31.0	39.5	27.8	14.5	10.2	24.5	29.8	21.8	6.0
3.5	0.0	0.0	0.0	1.3	14.1	16.6	21.9	16.0	11.4	18.9	17.7	14.8	4.3
4.0	0.0	0.0	0.0	0.0	4.0	5.2	27.8	23.0	7.0	14.5	14.9	10.9	3.3
4.5	0.0	0.0	0.0	0.0	0.0	3.0	11.6	7.6	8.9	21.5	22.1	8.4	0.0
5.0	0.0	0.0	0.0	0.0	0.0	0.0	6.5	5.6	6.0	16.9	23.3	14.2	2.2
5.5	0.0	0.0	0.0	0.0	0.0	0.0	4.7	4.0	12.6	21.1	12.6	5.1	1.3
6.0	0.0	0.0	0.0	0.0	0.0	0.0	3.7	3.2	2.9	5.6	5.7	4.8	1.6
6.5	0.0	0.0	0.0	0.0	0.0	0.0	1.1	0.9	1.7	4.1	6.7	7.2	2.5
7.0	0.0	0.0	0.0	0.0	0.0	0.0	0.0	0.0	2.0	2.8	1.9	8.3	5.8

Table 5
Energy output matrix (MWh) obtained for OEBuoy and location B4, considering local measurements.

	T_p (s)												
H_{m0} (m)	**4**	**5**	**6**	**7**	**8**	**9**	**10**	**11**	**12**	**13**	**14**	**15**	**16**
1.0	1.0	3.0	4.4	6.6	13.4	15.6	12.9	8.4	3.6	0.9	0.3	0.2	0.0
1.5	1.7	10.8	19.2	19.8	35.3	56.9	49.5	29.9	15.0	4.8	1.5	0.9	0.4
2.0	0.7	7.9	21.4	28.6	36.5	48.8	56.1	48.9	23.8	5.8	2.0	1.4	0.2
2.5	0.0	2.9	13.1	37.5	51.8	40.1	44.1	49.4	32.4	9.3	2.5	1.9	1.4
3.0	0.0	1.0	9.2	34.9	55.2	39.2	32.0	37.2	28.6	13.0	8.0	5.8	1.3
3.5	0.0	0.0	1.7	15.6	34.3	24.9	16.9	23.0	20.2	10.1	6.8	4.2	0.5
4.0	0.0	0.0	0.2	4.1	16.6	17.9	16.2	23.4	20.7	11.4	8.2	4.5	0.5
4.5	0.0	0.0	0.0	1.3	5.7	12.5	16.8	22.4	17.3	5.5	4.0	2.7	0.0
5.0	0.0	0.0	0.0	0.0	1.4	5.1	9.1	20.0	25.3	15.9	8.9	4.3	0.4
5.5	0.0	0.0	0.0	0.0	1.7	4.5	3.9	4.0	15.0	17.6	12.6	6.8	0.0
6.0	0.0	0.0	0.0	0.0	0.0	1.1	4.7	14.3	17.9	11.1	5.7	2.0	0.0
6.5	0.0	0.0	0.0	0.0	0.0	0.0	3.3	4.7	3.4	4.1	4.2	1.6	0.0
7.0	0.0	0.0	0.0	0.0	0.0	0.0	5.1	8.7	5.9	1.9	3.9	3.7	3.6

Table 6
The difference in energy outputs of measurements against SWAN (HWANG35) outputs for 8513 h time duration in location B4, in MWh for OEBuoy.

	T_p (s)												
H_{m0} (m)	**4**	**5**	**6**	**7**	**8**	**9**	**10**	**11**	**12**	**13**	**14**	**15**	**16**
1.0	−0.7	−1.6	−1.4	−1.8	−8.2	−8.1	−1.9	−2.8	−1.8	1.3	0.3	−0.2	0.0
1.5	−1.4	−5.0	−3.0	1.5	−9.1	−9.6	37.1	19.6	5.2	22.5	9.9	4.0	0.7
2.0	−0.7	−6.3	−11.8	−5.1	0.7	−3.6	32.3	8.8	8.3	42.1	18.8	3.6	1.2
2.5	0.0	−2.6	−9.1	−22.1	−15.2	−3.9	1.5	−19.2	−14.7	29.9	24.7	5.5	1.1
3.0	0.0	−1.0	−8.1	−29.3	−24.2	0.3	−4.2	−22.7	−18.4	11.5	21.8	16.0	4.7
3.5	0.0	0.0	−1.7	−14.3	−20.2	−8.3	5.1	−7.0	−8.8	8.7	10.9	10.6	3.8
4.0	0.0	0.0	−0.2	−4.1	−12.5	−12.7	11.6	−0.4	−13.7	3.1	6.7	6.4	2.8
4.5	0.0	0.0	0.0	−1.3	−5.7	−9.5	−5.3	−14.8	−8.5	16.0	18.1	5.7	0.0
5.0	0.0	0.0	0.0	0.0	−1.4	−5.1	−2.6	−14.4	−19.4	1.0	14.4	9.9	1.8
5.5	0.0	0.0	0.0	0.0	−1.7	−4.5	0.8	0.0	−2.4	3.5	0.0	−1.7	1.3
6.0	0.0	0.0	0.0	0.0	0.0	−1.1	−0.9	−11.1	−15.0	−5.6	0.0	2.7	1.6
6.5	0.0	0.0	0.0	0.0	0.0	0.0	−2.2	−3.7	−1.7	0.0	2.5	5.6	2.5
7.0	0.0	0.0	0.0	0.0	0.0	0.0	−5.1	−8.7	−3.9	0.9	−1.9	4.6	2.2

important to assess its energy output for local sea states obtained for different SWAN settings.

The present study investigated the uncertainty analysis of AEP due to simulated wave climate. The uncertainty in AEP estimation is a crucial problem in deploying WECs. Previous works have dealt with this issue from various aspects. Livermore [22] proposed a method for AEP uncertainty analysis based on standard error propagation, similar to the approach used in the wind energy industry. He identified four sources of AEP uncertainty: measurement uncertainty, temporal extrapolation uncertainty, spatial extrapolation uncertainty, and device performance uncertainty. Guanche et al. [23] used a boot-strap resampling technique to investigate the sensitivity of economic metrics to the variability in the wave climate, while Mackay et al. [24] investigated the impact of sampling variability on WEC performance uncertainty. Kofoed et al. [25] provided a method for estimating the uncertainty in AEP associated with device performance uncertainty, and Bailey et al. [26] used a numerical model of a self-reacting point absorber within a Monte Carlo simulation to investigate the variability in WEC power production within a single H_{m0}-T_e bin. The researchers observed a standard deviation in power production that amounts to 26% of the mean during their experiment. They concluded that the primary cause of this variability is the variation in wave conditions within the bin. However, the uncertainty in the AEP estimates related to the wave climate hindcast uncertainty was not evaluated.

5. Conclusions

In recent years, there has been a growing interest in exploiting wave

Table 7
The total energy output of OEBuoy (in MWh) for 10 different locations in the study area and 9 different SWAN settings against matched measurements for every location. The best estimations are highlighted in blue text.

Location	T (YEAR)	ECMWF32	ECMWF35	FAN28	FAN32	FAN35	HWANG32	HWANG35	ST6-DEF	SWAN-DEF	REAL-MEAS
B1	0.57	1739.75	1837.95	1590.32	1706.64	1797.97	1800.45	**1923.65**	1802.56	1778.03	1996.92
B2	0.30	854.56	957.80	713.98	828.99	**908.62**	909.79	1034.53	910.55	864.03	905.11
B3	0.25	621.94	682.07	534.96	**599.54**	656.57	658.45	730.29	663.08	624.83	598.55
B4	0.97	1539.37	1650.29	1391.87	1506.09	1605.19	1612.62	**1742.31**	1608.97	1595.78	1775.62
B5	0.69	1196.68	1307.47	1069.18	1168.83	1259.26	1265.26	**1392.66**	1264.63	1200.57	1299.50
B6	0.57	1764.59	1874.70	1620.88	1736.77	1828.99	1835.86	**1974.70**	1836.26	1811.58	2039.11
B7	1.00	3173.44	3404.79	2805.97	3067.02	3322.80	3332.78	**3588.56**	3326.08	3163.15	3558.74
B8	0.13	405.35	436.59	364.89	**395.21**	427.54	426.92	461.46	428.15	413.21	382.47
B9	0.78	731.04	804.22	624.75	698.56	774.29	777.89	**867.58**	780.15	768.70	884.35
B10	0.29	588.71	631.28	522.30	574.01	613.49	611.62	676.31	616.51	**596.22**	602.10
Mean	**0.56**	**1261.54**	**1358.72**	**1123.91**	**1228.17**	**1319.47**	**1323.16**	1439.21	**1323.69**	**1281.61**	**1404.25**

Table 8
Energy output difference in percentage (%) of OEBuoy for 10 different locations and 9 different SWAN settings against measurements. The difference percentages are color-scaled for every row separately (the closest values to zero are in green and the farthest values are in red). The closest value to zero represents the best model setting.

Location	T (YEAR)	ECMWF32	ECMWF35	FAN28	FAN32	FAN35	HWANG32	HWANG35	ST6-DEF	SWAN-DEF
B1	0.57	-12.88	-7.96	-20.36	-14.54	-9.96	-9.84	**-3.67**	-9.73	-10.96
B2	0.30	-5.58	5.82	-21.12	-8.41	**0.39**	0.52	14.30	0.60	-4.54
B3	0.25	3.91	13.95	-10.62	**0.16**	9.69	10.01	22.01	10.78	4.39
B4	0.97	-13.31	-7.06	-21.61	-15.18	-9.60	-9.18	**-1.88**	-9.39	-10.13
B5	0.69	-7.91	**0.61**	-17.72	-10.06	-3.10	-2.63	7.17	-2.68	-7.61
B6	0.57	-13.46	-8.06	-20.51	-14.83	-10.30	-9.97	**-3.16**	-9.95	-11.16
B7	1.00	-10.83	-4.33	-21.15	-13.82	-6.63	-6.35	**0.84**	-6.54	-11.12
B8	0.13	5.98	14.15	-4.60	**3.33**	11.79	11.62	20.66	11.94	8.04
B9	0.78	-17.34	-9.06	-29.35	-21.01	-12.44	-12.04	**-1.90**	-11.78	-13.08
B10	0.29	-2.22	4.85	-13.25	-4.66	1.89	1.58	12.33	2.39	**-0.98**
Mean	**0.56**	**-10.16**	**-3.24**	**-19.96**	**-12.54**	**-6.04**	**-5.77**	**2.49**	**-5.74**	**-8.73**

Table 9
Energy output difference in percentage (%) of WaveBob for 10 different locations and 9 different SWAN settings against measurements. The difference percentages are color-scaled for every row separately (the closest values to zero are in green and the farthest values are in red). The closest value to zero represents the best model setting.

Location	T (YEAR)	ECMWF32	ECMWF35	FAN28	FAN32	FAN35	HWANG32	HWANG35	ST6-DEF	SWAN-DEF
B1	0.57	-14.86	-10.72	-21.71	-16.28	-12.40	-12.31	**-7.02**	-12.23	-12.91
B2	0.30	-3.46	7.97	-17.78	-6.68	**2.38**	2.66	16.58	2.70	-2.74
B3	0.25	5.38	14.96	**-7.50**	**1.65**	10.81	11.01	22.19	11.71	6.38
B4	0.97	-10.63	-5.23	-17.75	-12.12	-7.11	-7.04	**-0.80**	-7.11	-7.07
B5	0.69	-4.69	2.89	-13.15	-6.43	-0.12	0.06	8.50	**0.01**	-3.72
B6	0.57	-15.57	-11.14	-22.02	-16.85	-13.00	-12.72	**-6.97**	-12.69	-13.44
B7	1.00	-9.09	-2.85	-18.63	-11.89	-5.30	-5.03	**2.04**	-5.20	-9.26
B8	0.13	8.40	15.96	**-1.45**	6.17	14.01	13.72	21.58	14.09	9.33
B9	0.78	-14.07	-7.03	-24.54	-17.24	-10.10	-9.80	**-0.63**	-9.47	-10.21
B10	0.29	-2.57	3.20	-11.79	-4.50	0.88	**0.63**	9.61	1.25	-0.93
Mean	**0.56**	**-9.21**	**-2.98**	**-18.01**	**-11.36**	**-5.51**	**-5.34**	**2.16**	**-5.28**	**-7.68**

energy as a potential renewable energy source. To that end, a large number of studies have been conducted to assess the wave potential through numerical modeling. However, many of these studies offer only a rough estimation of wave resources due to the challenges faced in implementing the model. One such challenge is the lack of available data for forcing and calibrating the numerical model in the area of interest.

This study aimed to assess the influence of different numerical set-up parameters for the spectral wave model SWAN (ST6 physics package) on the uncertainty of the energy production of three case-study WECs – OEBuoy, WaveBob, and Pontoon – at 10 different areas along the Atlantic coast of the Iberian Peninsula. To calibrate the model, the study considered different wind drag formulations and wind scaling factors of the SWAN-ST6 package.

The study found that the HWANG wind drag formulation and a wind scaling factor of 35 provided the best validation results. Regarding the estimation of the energy production of the three case-study WECs, the study found that adjustments to the SWAN model resulted in a maximum observed difference in energy production for OEBuoy in location B9, ranging between −29.35% (FAN28) and −1.90% (HWANG35); for WaveBob in location B2, ranging between −17.78% (FAN28) and +16.58% (HWANG35); and for Pontoon in location B2, ranging between −27.93% (FAN28) and +7.84% (HWANG35).

The study concluded that there is remarkable uncertainty in the estimated energy production of the three case-study WECs. The calibrated model corrected the mean energy output value of all 10 locations: 11.22% for OEBuoy, 9.84% for WaveBob, and 10.87% for Pontoon, compared to the SWAN default settings. The uncertainty may be due to the lower accuracy of T_p estimations in the SWAN model compared to

Table 10
Energy output difference in percentage (%) of Pontoon for 10 different locations and 9 different SWAN settings against measurements. The difference percentages are color-scaled for every row separately (the closest values to zero are in green and the farthest values are in red). The closest value to zero represents the best model setting.

Location	T (YEAR)	ECMWF32	ECMWF35	FAN28	FAN32	FAN35	HWANG32	HWANG35	ST6-DEF	SWAN-DEF
B1	0.57	-30.57	-25.94	-37.41	-32.00	-27.81	-27.52	**-22.37**	-27.45	-30.37
B2	0.30	-11.52	**-0.07**	-27.93	-14.68	-5.70	-5.34	7.84	-5.27	-12.50
B3	0.25	-6.65	2.06	-19.83	-9.24	-1.06	-0.59	9.15	**-0.37**	-7.88
B4	0.97	-20.63	-15.85	-26.99	-21.57	-17.41	-17.28	**-12.05**	-17.32	-18.49
B5	0.69	-17.19	-10.80	-24.31	-18.67	-13.43	-13.18	**-6.76**	-13.17	-18.23
B6	0.57	-30.59	-25.81	-37.60	-32.09	-27.83	-27.58	**-21.68**	-27.55	-30.51
B7	1.00	-23.09	-16.92	-32.93	-25.76	-19.47	-18.88	**-12.63**	-19.12	-24.43
B8	0.13	**-0.56**	7.70	-10.54	-3.50	5.34	5.43	13.79	5.73	-0.97
B9	0.78	-24.77	-18.63	-34.99	-26.97	-20.32	-20.24	**-12.45**	-20.26	-21.52
B10	0.29	-3.87	4.11	-13.75	-6.26	0.95	**0.68**	11.53	1.07	-3.04
Mean	**0.56**	**-21.44**	**-15.24**	**-30.35**	**-23.42**	**-17.68**	**-17.38**	**-10.49**	**-17.40**	**-21.36**

Table 11
Comparison of the usual calibrated SWAN model with the calibration settings suggested by considering the case study WECs for 10 different locations in the study area.

Location	T (Year)	Best model settings			
		Calibration	OEBuoy output	WaveBob output	Pontoon output
B1	0.57	HWANG35	HWANG35	HWANG35	HWANG35
B2	0.30	HWANG35	FAN35	FAN35	ECMWF35
B3	0.25	HWANG35	FAN32	FAN32	ST6-DEF
B4	0.97	HWANG35	HWANG35	HWANG35	HWANG35
B5	0.69	FAN35	ECMWF35	ST6-DEF	HWANG35
B6	0.57	HWANG35	HWANG35	HWANG35	HWANG35
B7	1.00	FAN35	HWANG35	HWANG35	HWANG35
B8	0.13	FAN35	FAN32	FAN28	ECMWF32
B9	0.78	HWANG35	HWANG35	HWANG35	HWANG35
B10	0.29	HWANG35	SWAN-DEF	HWANG32	HWANG32

T_{m02} and T_e. Therefore, the study suggested that a power matrix, which is a function of T_{m02} or T_e, may reduce the uncertainty in the estimation of the electricity production of a WEC.

Furthermore, the study suggests that various SWAN adjustments may be necessary for different locations. The estimated energy outputs for the three case-study WECs highlight the importance of assessing the AEP of WECs using output data from different model settings while implementing WEC technology. It is crucial to optimize WECs for each location of interest, as WEC technologies perform differently in different areas. Doing so may help to reduce uncertainty and enhance the quality of a WEC energy output estimation.

Author contributions

Ajab Gul Majidi: Conceptualization, Investigation, Software, Formal analysis, Data curation, Visualization, Writing - original draft. **Victor Ramos**: Software, Methodology, Data curation, Visualization, Writing - review & editing. **Khalid Amarouche**: Conceptualization, Software, Data curation. **Paulo Rosa Santos**: Conceptualization, Methodology, Writing - review & editing, Supervision, Funding acquisition. **Luciana das Neves**: Writing - review & editing, Supervision, Funding acquisition. **Francisco Taveira-Pinto**: Writing - review & editing, Supervision, Funding acquisition.

Declaration of competing interest

The authors declare that they have no known competing financial interests or personal relationships that could have appeared to influence the work reported in this paper.

Data availability

The data that has been used is confidential.

Acknowledgments

The authors would like to express their gratitude to Prof. Dr. Adem AKPINAR for his invaluable support and guidance throughout this research study. The authors also acknowledge funding in the form of a Ph.D. scholarship grant by the FCT, co-financed by the EU's ESF through the NORTE 2020 program, with reference 2021.04847.BD. This work was also supported by the project WEC4Ports – A hybrid Wave Energy Converter for Ports (OCEANERA-NET COFUND, with the reference OCEANERA/0004/2019) funded under the frame of FCT, and the project ATLANTIDA (NORTE-01-0145-FEDER-000040), supported by the North Portugal Regional Operational Programme (NORTE2020), under the PORTUGAL 2020 Partnership Agreement and through the European Regional Development Fund (ERDF). Furthermore, during this research study, Victor Ramos was supported by the program of Stimulus of Scientific Employment Individual Support (CEECIND/03665/2018) from the Portuguese Foundation of Science and Technology (FCT).

Appendix A. The power matrices of the considered WECs

Table A.1
The Power matrix for the full scale of the OEBuoy wave energy converter (kW).

		TP (s)												
		4	5	6	7	8	9	10	11	12	13	14	15	16
H_{m0} (m)	**1.0**	8	17	27	42	56	59	52	44	40	38	40	38	30
	1.5	17	39	61	96	126	132	117	99	89	87	89	85	66
	2.0	30	69	108	170	224	235	208	177	159	154	159	151	118
	2.5	47	108	169	266	350	368	324	276	249	241	248	236	185

(*continued on next page*)

Table A.1 (*continued*)

		TP (s)												
		4	5	6	7	8	9	10	11	12	13	14	15	16
	3.0	68	155	244	383	504	530	467	398	358	347	357	340	266
	3.5	93	212	332	521	686	721	636	542	487	472	486	463	362
	4.0	121	276	433	680	896	942	831	708	636	616	634	605	473
	4.5	154	350	548	861	1130	1190	1050	896	805	780	803	765	599
	5.0	190	432	677	1060	1400	1470	1300	1110	994	963	991	945	739
	5.5	0	523	819	1290	1690	1780	1570	1340	1200	1170	1200	1140	894
	6.0	0	622	975	1530	2020	2120	1870	1590	1430	1390	1430	1360	1060
	6.5	0	730	1140	1800	2370	2490	2190	1870	1680	1630	1670	1600	1250
	7.0	0	847	1330	2080	2750	2880	2540	2170	1950	1890	1940	1850	1450

Table A.2
The Power matrix for the full scale of the WaveBob wave energy converter (kW).

		TP (s)												
		4	5	6	7	8	9	10	11	12	13	14	15	16
H_{m0} **(m)**	**1.0**	6	11	19	25	30	44	50	53	44	34	22	20	17
	1.5	13	25	43	55	68	90	102	92	91	66	65	65	45
	2.0	24	45	65	100	121	153	175	151	122	126	87	61	58
	2.5	0	65	104	141	191	179	243	255	190	181	135	99	83
	3.0	0	96	137	205	244	357	293	353	260	248	184	137	120
	3.5	0	0	192	254	291	431	385	424	324	285	239	222	172
	4.0	0	0	256	366	403	551	536	531	473	420	289	268	179
	4.	0	0	327	418	574	678	708	665	509	415	386	244	249
	5.0	0	0	358	514	658	824	828	618	638	512	453	384	333
	5.5	0	0	0	610	774	880	936	905	805	603	456	397	311
	6.0	0	0	0	711	952	974	1000	838	886	648	501	503	396
	6.5	0	0	0	788	1000	1000	1000	979	1000	727	577	435	424
	7.0	0	0	0	871	1000	1000	1000	1000	1000	959	748	574	478

Table A.3
The Power matrix for the full scale of the Pontoon wave energy converter (kW).

		TP (s)												
		4	5	6	7	8	9	10	11	12	13	14	15	16
H_{m0} **(m)**	**1.0**	180	166	153	171	125	87	72	65	85	85	37	29	16
	1.5	223	195	157	148	261	192	223	139	155	155	74	67	46
	2.0	0	0	214	227	396	335	237	235	172	138	115	104	70
	2.5	0	0	0	440	598	514	379	342	204	169	142	128	95
	3.0	0	0	0	681	801	735	594	486	199	174	151	134	121
	3.5	0	0	0	904	1035	949	788	617	239	209	183	164	146
	4.0	0	0	0	1131	1269	1163	982	743	285	248	216	195	175
	4.5	0	0	0	1358	1488	1374	1187	869	330	287	250	225	201
	5.0	0	0	0	1585	1712	1585	1392	988	380	334	285	263	226
	5.5	0	0	0	1812	1937	1798	2138	1107	429	381	323	301	261
	6.0	0	0	0	2040	2162	2010	2884	1234	439	416	361	336	295
	6.5	0	0	0	2267	2386	2221	3143	1360	449	450	406	372	329
	7.0	0	0	0	2494	2611	2433	3619	1483	506	464	451	408	363

Appendix B. The definition of the statistical error parameters considered in the study

Because merely one or two statistical error parameters might lead to a misinterpretation of a model's results, it is vital to use a combination of different statistical error methods to make a proper judgment on the quality of a model. So, MAE, RMSE, bias, SI, and correlation coefficient, are utilized to verify the outputs of the model. Eq. (B.1) is used for the computation of the mean absolute error (MAE) [34,35].

$$MAE = \frac{1}{n}\sum_{i=1}^{n}|Y_i - X_i| \tag{B.1}$$

Where Y_i represents the model output values, X_i is the observation values and n is the number of the temporally matched data. The root-mean-square error (*RMSE*) is computed by Eq. (B.2).

$$RMSE = \sqrt{\frac{1}{n}\sum_{i=1}^{n}(X_i - Y_i)^2} \tag{B.2}$$

The variables in Eq. B.2 are the same as in Eq. B.1. *BIAS*, the mean difference is calculated by Eq. (B.3).

$$BIAS = (\overline{X} - \overline{Y}) \tag{B.3}$$

Where $\overline{X}$ and $\overline{Y}$ are the mean values of the measurements and model, respectively, the scatter index *SI* is also calculated using Eq. (B.4).

$$SI = \frac{RMSE}{\overline{X}} \tag{B.4}$$

The closest value to zero represents greater performance for all of the considered error indices. Eq. (B.5) calculates the correlation coefficient (*R*) demonstrating the connection between the model dataset and measurements.

$$R = \frac{\sum_{i=1}^{n}(X_i - \overline{X})(Y_i - \overline{Y})}{\sqrt{\sum_{i=1}^{n}(X_i - \overline{X})^2 \sum_{i=1}^{n}(Y_i - \overline{Y})^2}} \tag{B.5}$$

References

[1] Communication from the Commission to the European Parliament, the European Council, the Council, the European Economic and Social Committee and the Committee of the Regions, 2019. https://www.eea.europa.eu/policy-documents/com-2019-640-final. (Accessed 11 January 2022).

[2] V. Ramos, G. Giannini, T. Calheiros-Cabral, P. Rosa-Santos, F. Taveira-Pinto, Legal framework of marine renewable energy: a review for the Atlantic region of Europe, Renew. Sustain. Energy Rev. 137 (2021), 110608, https://doi.org/10.1016/J.RSER.2020.110608.

[3] F. Taveira-Pinto, P. Rosa-Santos, T. Fazeres-Ferradosa, Marine renewable energy, Renew. Energy 150 (2020) 1160–1164, https://doi.org/10.1016/J.RENENE.2019.10.014.

[4] A.S. Bahaj, Generating electricity from the oceans, Renew. Sustain. Energy Rev. 15 (2011) 3399–3416, https://doi.org/10.1016/J.RSER.2011.04.032.

[5] K. Gunn, C. Stock-Williams, Quantifying the global wave power resource, Renew. Energy 44 (2012) 296–304, https://doi.org/10.1016/J.RENENE.2012.01.101.

[6] V. Ramos, G. Giannini, T. Calheiros-Cabral, P. Rosa-Santos, F. Taveira-Pinto, An integrated approach to assessing the wave potential for the energy supply of Ports: a case study, J. Mar. Sci. Eng. 10 (2022) 1989, https://doi.org/10.3390/JMSE10121989, 10 (2022) 1989.

[7] R. Carballo, N. Arean, M. Álvarez, I. López, A. Castro, M. López, G. Iglesias, Wave farm planning through high-resolution resource and performance characterization, Renew. Energy 135 (2019) 1097–1107, https://doi.org/10.1016/J.RENENE.2018.12.081.

[8] N. Arean, R. Carballo, G. Iglesias, An integrated approach for the installation of a wave farm, Energy 138 (2017) 910–919, https://doi.org/10.1016/J.ENERGY.2017.07.114.

[9] K. Amarouche, A. Akpınar, N.E.I. Bachari, R.E. Çakmak, F. Houma, Evaluation of a high-resolution wave hindcast model SWAN for the West Mediterranean basin, Appl. Ocean Res. 84 (2019) 225–241, https://doi.org/10.1016/j.apor.2019.01.014.

[10] A. Akpınar, B. Bingölbali, G.P. Van Vledder, Long-term analysis of wave power potential in the Black Sea, based on 31-year SWAN simulations, Ocean Eng. 130 (2017) 482–497, https://doi.org/10.1016/j.oceaneng.2016.12.023.

[11] B. Bingölbali, A.G. Majidi, A. Akpınar, Inter- and intra-annual wave energy resource assessment in the south-western Black Sea coast, Renew. Energy 169 (2021) 809–819, https://doi.org/10.1016/J.RENENE.2021.01.057.

[12] A.A. Abu Zed, R.M. Kansoh, M.M. Iskander, M. Elkholy, Wind and wave climate southeastern of the Mediterranean Sea based on a high-resolution SWAN model, Dynam. Atmos. Oceans 99 (2022), 101311, https://doi.org/10.1016/J.DYNATMOCE.2022.101311.

[13] W. Wu, Z. Liu, F. Zhai, P. Li, Y. Gu, K. Wu, A quantitative method to calibrate the SWAN wave model based on the whitecapping dissipation term, Appl. Ocean Res. 114 (2021), 102785, https://doi.org/10.1016/J.APOR.2021.102785.

[14] B. Aydoğan, B. Ayat, Performance evaluation of SWAN ST6 physics forced by ERA5 wind fields for wave prediction in an enclosed basin, Ocean Eng. 240 (2021), 109936, https://doi.org/10.1016/J.OCEANENG.2021.109936.

[15] P.A. Hwang, A note on the ocean surface roughness spectrum, J. Atmos. Ocean. Technol. 28 (2011) 436–443, https://doi.org/10.1175/2010JTECHO812.1.

[16] Y. Fan, S.J. Lin, I.M. Held, Z. Yu, H.L. Tolman, Global Ocean surface wave simulation using a coupled atmosphere–wave model, J. Clim. 25 (2012) 6233–6252, https://doi.org/10.1175/JCLI-D-11-00621.1.

[17] T.W. Group, The WAM model—a third generation ocean wave prediction model, J. Phys. Oceanogr. 18 (1988) 1775–1810, https://doi.org/10.1175/1520-0485(1988)018.

[18] SWAN team, SWAN User Manual, Delft University of Technology, the Netherlands, 2006.

[19] W. Erick Rogers, A.V. Babanin, D.W. Wang, Observation-consistent input and whitecapping dissipation in a model for wind-generated surface waves: description and simple calculations, J. Atmos. Ocean. Technol. 29 (2012) 1329–1346, https://doi.org/10.1175/JTECH-D-11-00092.1.

[20] EMEC Standards, European marine energy Centre. https://www.emec.org.uk/standards/. (Accessed 6 June 2022).

[21] C.E. Hiles, S.J. Beatty, A. de Andres, Wave energy converter annual energy production uncertainty using simulations, J. Mar. Sci. Eng. 4 (2016) 53, https://doi.org/10.3390/JMSE4030053, 4 (2016) 53.

[22] Livermore: wave and tidal energy yield uncertainty - google scholar, n.d. https://scholar.google.com/scholar_lookup?title=Wave+and+Tidal+Energy+Yield+Uncertainty&author=Livermore,+S.&publication_year=2015. (Accessed 28 February 2022).

[23] R. Guanche, A.D. de Andrés, P.D. Simal, C. Vidal, I.J. Losada, Uncertainty analysis of wave energy farms financial indicators, Renew. Energy 68 (2014) 570–580, https://doi.org/10.1016/J.RENENE.2014.02.046.

[24] E.B. Mackay, Wave Energy Resource Assessment, University of Southampton, 2009. Doctoral dissertation.

[25] J.P. Kofoed, A. Pecher, L. Margheritini, M. Antonishen, C. Bittencourt, B. Holmes, C. Retzler, K. Berthelsen, I. le Crom, F. Neumann, C. Johnstone, T. McCombes, L. E. Myers, A methodology for equitable performance assessment and presentation of wave energy converters based on sea trials, Renew. Energy 52 (2013) 99–110, https://doi.org/10.1016/J.RENENE.2012.10.040.

[26] H. Bailey, B. Robertson, B. Buckham, Quantifying and discritizing the uncertainity in the power production estimates of a wave energy converter, in: Proceedings of the 4th Annual Marine Energy Technology Symposium, METS), Washington, DC, USA, 2016, April, pp. 25–27.

[27] Iec, IEC/TS 62600-100 Marine Energy-Wave, Tidal and Other Water Current Converters-Part 100: Electricity Producing Wave Energy Converters-Power Performance Assessment, 2012.

[28] V. Ramos, J.v. Ringwood, Exploring the utility and effectiveness of the IEC (International Electrotechnical Commission) wave energy resource assessment and characterisation standard: a case study, Energy 107 (2016) 668–682, https://doi.org/10.1016/J.ENERGY.2016.04.053.

[29] A. Mérigaud, J.v. Ringwood, Power Production Assessment for Wave Energy Converters: Overcoming the Perils of the Power Matrix, 2018, pp. 50–70, https://doi.org/10.1177/1475090217731671, 10.1177/1475090217731671. 232.

[30] M. Dhi, MIKE 21 Spectral Wave Module, Scientific Documentation, DHI Water Environment Health, Hørsholm, Denmark, 2017.

[31] TOMAWAC - wave propagation in coastal areas. http://www.opentelemac.org/index.php/presentation?id=20. (Accessed 17 July 2022).

[32] H.L. Tolman, User manual and system documentation of WAVEWATCH III TM version 3.14. Technical note, MMAB Contribution (220) (2009) 276.

[33] H. Günther, S. Hasselmann, P.A. Janssen, The WAM Model Cycle 4, 1992.

[34] A.G. Majidi, B. Bingölbali, A. Akpınar, E. Rusu, Wave power performance of wave energy converters at high-energy areas of a semi-enclosed sea, Energy 220 (2021), 119705, https://doi.org/10.1016/J.ENERGY.2020.119705.

[35] A.G. Majidi, B. Bingölbali, A. Akpınar, G. Iglesias, H. Jafali, Downscaling wave energy converters for optimum performance in low-energy seas, Renew. Energy 168 (2021) 705–722, https://doi.org/10.1016/J.RENENE.2020.12.092.

[36] V. Ramos, M. López, F. Taveira-Pinto, P. Rosa-Santos, Influence of the wave climate seasonality on the performance of a wave energy converter: a case study, Energy 135 (2017) 303–316, https://doi.org/10.1016/J.ENERGY.2017.06.080.

[37] V. Ramos, M. López, F. Taveira-Pinto, P. Rosa-Santos, Performance assessment of the CECO wave energy converter: water depth influence, Renew. Energy 117 (2018) 341–356, https://doi.org/10.1016/J.RENENE.2017.10.064.

[38] D. Silva, P. Martinho, C. Guedes Soares, Wave energy distribution along the Portuguese continental coast based on a thirty three years hindcast, Renew. Energy 127 (2018) 1064–1075, https://doi.org/10.1016/J.RENENE.2018.05.037.

[39] L. Castro-Santos, D. Silva, A.R. Bento, N. Salvação, C.G. Soares, Economic feasibility of wave energy farms in Portugal, Energies 11 (2018) 3149, https://doi.org/10.3390/EN11113149, 11 (2018) 3149.

[40] A. Akpınar, B. Bingölbali, G.Ph Van Vledder, Wind and wave characteristics in the Black Sea based on the {SWAN} wave model forced with the {CFSR} winds, Ocean Eng. 126 (2016) 276–298, https://doi.org/10.1016/j.oceaneng.2016.09.026.

[41] K. Amarouche, A. Akpınar, R.E. Çakmak, F. Houma, N.E.I. Bachari, Assessment of storm events along the Algiers coast and their potential impacts, Ocean Eng. 210 (2020), 107432, https://doi.org/10.1016/j.oceaneng.2020.107432.
[42] B. Bingölbali, A. Akpınar, H. Jafali, G.P. Van Vledder, Downscaling of wave climate in the western Black Sea, Ocean Eng. 172 (2019) 31–45, https://doi.org/10.1016/J.OCEANENG.2018.11.042.
[43] P.A. Umesh, P.K. Bhaskaran, K.G. Sandhya, T.M. Balakrishnan Nair, An assessment on the impact of wind forcing on simulation and validation of wave spectra at coastal Puducherry, east coast of India, Ocean Eng. 139 (2017) 14–32, https://doi.org/10.1016/J.OCEANENG.2017.04.043.
[44] S. Myslenkov, A. Chernyshova, Comparing wave heights simulated in the Black Sea by the SWAN model with satellite data and direct wave measurements, Russ. J. Earth Sci. 16 (2016), https://doi.org/10.2205/2016ES000579.
[45] N. Booij, R.C. Ris, L.H. Holthuijsen, A third-generation wave model for coastal regions: 1. Model description and validation, J Geophys Res Oceans 104 (1999) 7649–7666, https://doi.org/10.1029/98JC02622.
[46] M.W. Dingemans, Water Wave Propagation over Uneven Bottoms, World Scientific Publishing Company, London, 1997, https://doi.org/10.1142/1241.
[47] G.B. Whitham, T.C.T. Ting, Linear and nonlinear waves, J. Appl. Mech. 43 (1976) 190, https://doi.org/10.1115/1.3423786. –190.
[48] M. Zijlema, Computation of wind-wave spectra in coastal waters with SWAN on unstructured grids, Coast. Eng. 57 (2010) 267–277, https://doi.org/10.1016/j.coastaleng.2009.10.011.
[49] SWAN Team, Swan Scientific and Technical Documentation, Swan Cycle Iii Version SWAN, Scientific and Technical Documentation, 2020. SWAN Cycle III version 41.31A.
[50] S. Aijaz, W.E. Rogers, A.V. Babanin, Wave spectral response to sudden changes in wind direction in finite-depth waters, Ocean Model. 103 (2016) 98–117, https://doi.org/10.1016/J.OCEMOD.2015.11.006.
[51] I.R. Young, A.V. Babanin, Spectral distribution of energy dissipation of wind-generated waves due to dominant wave breaking, J. Phys. Oceanogr. 36 (2006) 376–394, https://doi.org/10.1175/JPO2859.1.
[52] M.A. Donelan, A.V. Babanin, I.R. Young, M.L. Banner, M.A. Donelan, A.V. Babanin, I.R. Young, M.L. Banner, Wave-follower field measurements of the wind-input spectral function. Part II: parameterization of the wind input, J. Phys. Oceanogr. 36 (2006) 1672–1689, https://doi.org/10.1175/JPO2933.1.
[53] SWAN ST6 Physics. https://swanmodel.sourceforge.io/online_doc/swanuse/node28.html. (Accessed 3 May 2023).
[54] F. Ardhuin, A. Roland, The development of spectral wave models: coastal and coupled aspects, in: Proceedings of Coastal Dynamics, vol. 2013, 2013, June, p. 7.
[55] H. Hersbach, B. Bell, P. Berrisford, G. Biavati, A. Horányi, J. Muñoz Sabater, J. N. Thépaut, ERA5 hourly data on single levels from 1979 to present, Copernicus climate change service (c3s) climate data store (cds) 10 (10) (2018) 24381.
[56] H. Hersbach, B. Bell, P. Berrisford, S. Hirahara, A. Horányi, J. Muñoz-Sabater, J. Nicolas, C. Peubey, R. Radu, D. Schepers, A. Simmons, C. Soci, S. Abdalla, X. Abellan, G. Balsamo, P. Bechtold, G. Biavati, J. Bidlot, M. Bonavita, G. De Chiara, P. Dahlgren, D. Dee, M. Diamantakis, R. Dragani, J. Flemming, R. Forbes, M. Fuentes, A. Geer, L. Haimberger, S. Healy, R.J. Hogan, E. Hólm, M. Janisková, S. Keeley, P. Laloyaux, P. Lopez, C. Lupu, G. Radnoti, P. de Rosnay, I. Rozum, F. Vamborg, S. Villaume, J.N. Thépaut, The ERA5 global reanalysis, Q. J. R. Meteorol. Soc. 146 (2020) 1999–2049, https://doi.org/10.1002/QJ.3803.
[57] E.M. Dias, A. Cristi, N. Pinto, A. Palmeira, R. Libonati, Estimativa dos períodos de retorno da velocidade e rajada do vento e altura significativa das ondas no Atlântico Sudoeste, Sistemas & Gestão 16 (2021) 84–100, https://doi.org/10.20985/1980-5160.2021.V16N1.1703.
[58] A.A. Akinsanola, K.O. Ogunjobi, A.T. Abolude, S. Salack, Projected changes in wind speed and wind energy potential over West Africa in CMIP6 models, Environ. Res. Lett. 16 (2021), 044033, https://doi.org/10.1088/1748-9326/ABED7A.
[59] M.F. Bruno, M.G. Molfetta, V. Totaro, M. Mossa, Performance assessment of ERA5 wave data in a swell dominated region, J. Mar. Sci. Eng. 8 (2020) 214, https://doi.org/10.3390/JMSE8030214, 8 (2020) 214.
[60] D.A. Macleod, A. Jones, F. di Giuseppe, V. Sharmar, M. Markina, Validation of global wind wave hindcasts using ERA5, MERRA2, ERA-Interim and CFSRv2 reanalyzes, IOP Conf. Ser. Earth Environ. Sci. 606 (2020), 012056, https://doi.org/10.1088/1755-1315/606/1/012056.
[61] T. Wang, Z. Yang, W.C. Wu, M. Grear, A sensitivity analysis of the wind forcing effect on the accuracy of large-wave hindcasting, J. Mar. Sci. Eng. 6 (2018) 139, https://doi.org/10.3390/JMSE6040139, 6 (2018) 139.
[62] A. Akpınar, B. Bingölbali, Long-term variations of wind and wave conditions in the coastal regions of the Black Sea, Nat. Hazards 84 (2016) 69–92, https://doi.org/10.1007/S11069-016-2407-9/FIGURES/10.
[63] M.A. Hoque, W. Perrie, S.M. Solomon, Application of SWAN model for storm generated wave simulation in the Canadian Beaufort Sea, J. Ocean Eng. Sci. 5 (2020) 19–34, https://doi.org/10.1016/j.joes.2019.07.003.
[64] A. Mazzolari, Two Dimensional Unstructured Mesh Generation Applied to Shallow Water Models (Doctoral Dissertation, PhD Thesis, Department of Civil Engineering. Instituto Superior Técnico, Lisbon), 2013.
[65] D.C. Kapoor, General bathymetric chart of the oceans (GEBCO), Mar. Geodes. 5 (1) (1981) 73–80.
[66] K. Amarouche, A. Akpınar, M.B. Soran, S. Myslenkov, A.G. Majidi, M. Kankal, V. Arkhipkin, Spatial calibration of an unstructured SWAN model forced with CFSR and ERA5 winds for the Black and Azov Seas, Appl. Ocean Res. 117 (2021), 102962, https://doi.org/10.1016/J.APOR.2021.102962.
[67] N. Guillou, G. Chapalain, Annual and seasonal variabilities in the performances of wave energy converters, Energy 165 (2018) 812–823, https://doi.org/10.1016/J.ENERGY.2018.10.001.